RESEARCH ARTICLE

Employing $ZnFe_2O_4$ as a nano photocatalyst for degradation of Tert-Butyl alcohol in synthetic wastewater

Aref Shokri [1,2], Fariba Soleimani[3], Mahdi Sanavi Fard[4], Ali Hassani Joshaghani[5]*

[1]Jundi-Shapur Research Institute, Jundi-Shapur University of Technology, Dezful, Iran
[2]Department of Chemical Engineering, Amirkabir University of Technology, Tehran, Iran
[3]Razi Chemistry Research Center (RCRC), Shahreza Branch, Islamic Azad University, Isfahan, Iran
[4]Department of Chemical Engineering, Tafresh University, Tafresh, Iran
[5]Department of Chemical Engineering, Faculty of Technical Engineering, Arak Branch, Islamic Azad University, Arak, Iran

ARTICLE INFO

Article History:
Received 2021-07-17
Accepted 2022-0315
Published 2022-06-30

Keywords:
Tert- Butyl alcohol (TBA), Batch photoreactor, Langmuir-Hinshel wood model, Co-precipitation method, UV/ZnFe2O4 process.

ABSTRACT

The wastewater containing Tert- Butyl alcohol (TBA) contains water-soluble polymer discharged from different chemical and textile industries. In this study, through the application of the UV/$ZnFe_2O_4$ approach in a batch photoreactor, the decomposition of synthetic wastewater, including TBA was investigated. The co-precipitation method was utilized for synthesizing the $ZnFe_2O_4$ nano photocatalyst. Using FT-IR spectroscopy, XRD, and SEM images, the characterization of catalyst was ascertained. For evaluation and exploration of the stability of nano photocatalyst particles, the Zeta potential was utilized. The influence of different crucial factors including the concentration of the catalyst, the initial dosage of contaminants, and pH, on the mineralization of TBA was studied. At optimal situations (pH at 6, 25 mg/l of TBA, and 0.9 g/l of catalyst) and after 120 min of remediation time, around 58% of Chemical Oxygen Demand (COD) and 93.5% of TBA was eliminated. Main reason for the generation of active radicals in the photocatalytic method is the electron-hole mechanism. According to the Langmuir Hinshelwood model, the kinetic of the TBA decomposition was elucidated hence, the half-life of the reaction and the apparent rate of the pseudo-first-order reaction were obtained ($t_{1/2}$=35 min) and (K_{app}=1.98×10^{-2} min^{-1}), respectively.

How to cite this article
HassaniJoshaghani A., Soleimani F., Sanavi Fard M., Shokri A., Employing ZnFe2O4 as a nano photocatalyst for degradation of Tert- Butyl alcohol in synthetic wastewater. J. Nanoanalysis., 2022; 9(2): 148-158. DOI: 10.22034/jna.2022.1935754.1266.

INTRODUCTION

Tert-Butyl alcohol (TBA) is considered as a pollutant with the assumption that potentially could have a carcinogenic effect on human health. The existence of TBA in water has posed a significant challenge to the research community regarding finding methods for its effective remediation and decomposition [1]. It has some special physical characteristics such as lower inclination towards adsorption and lower Henry's constant in comparison with MTBE besides greater amounts of water solubility, which prevents its proper remediation through traditional methods. Generally, TBA has been utilized as a component in the synthesis of several chemical materials, different types of cosmetic productions, perfumes, industrial-scale cleaning constituents, and paint eliminators. Moreover, to increase octane number and decrease atmospheric emissions, TBA has been added to gasoline [2]. As a result, it is frequently detected in the sewage of plants that generate TBA. Moreover, for decomposition of other fuel oxygenates like ethyl tert-butyl ether (ETBE) and methyl tert-butyl ether (MTBE) it has been stated

* Corresponding Author Email: *aref.shokri3@gmail.com*

as a reliable intermediate [3].

To eliminate TBA from polluted water and wastewater sources, based on the previous investigations, remediation approaches like air stripping and adsorption with activated carbon are inefficient. It is worth mentioning that in comparison with MTBE, TBA has shown a lower inclination towards absorption on the surface of activated carbon. By application of air stripping technique in which considerable quantities of air and water are needed to achieve the appropriate effect, the TBA cannot be efficiently and conveniently eliminated because of its low Henry's constant. Moreover, in comparison with MTBE, the biological degradation of TBA is stated inefficient. As a result, the accumulation of TBA in groundwater is highly feasible [4]. The shortcoming of aforesaid traditional remediation approaches to efficient removal of the TBA has propelled the researchers towards investigating alternative techniques for mitigating such crucial challenges. In addition, Tert-butyl formate (TBF) is considered as the major intermediate generated throughout the advanced oxidation, chemical oxidation, and biological degradation of MTBE [5].

Several documents show the carcinogenic effect of TBA-polluted water samples, which indicates the toxic nature of such constituents and health hazards that stem from its existence in water. As a result, numerous treatment methods have been conducted regarding the remediation of aqueous TBA solutions to determine and assess its elimination status in the water [6-7]. Despite the lower remediation expenses of biological-driven treatment approaches, they need a somewhat time-prohibitive remediation process and have lower decomposition effectiveness for the remediation of such constituents. As an alternative, recently the significant reaction ratio of this constituent with $OH^{\cdot}$ has gained remarkable focus to the removal of TBA from water through the application of AOPs [8-10]. The working principles of AOPs are that various integrations of catalysts and reagents are utilized for the production of non-selective $OH^{\cdot}$ as powerful reagent to degradation of the pollutants in wastewater [11].

Biological processes cannot eliminate bio-resistant contaminants, and traditional remediation methods like adsorption, flocculation, and coagulation are not efficient since they produce useless solid disposal and only result in phase transformation of pollutant. In addition, they pose significant environmental hazards, hence the application of advanced oxidation processes (AOPs) will be of prime option. The mechanism of AOPs is such that, active free radicals like $OH^{\cdot}$ are generated, which possess significant oxidation potential for degradation of organic pollutants [12]. These non-selective radicals have enough power to react with organic compounds to achieve dehydrogenated or hydroxylated by-products until complete mineralization of contaminants to harmless products such as mineral ions, water, and carbon dioxide [13-14]. For this purpose, numerous methods such as chemical oxidation, adsorption, electrocoagulation, and biodegradation have been evolved. Time-prohibitive reactions and significant capital costs are some of the major limitations of chemical and biological methods.

Recently, the nanoparticles of $ZnFe_2O_4$ (nickel ferrite) have gained considerable focus due to their photocatalytic utilizations. Nickel ferrite is a soft magnetic substance with lower electrical resistance. In photocatalytic employments, the morphology and bandgap play pivotal functions [15]. Several procedures have been utilized to synthesize nickel ferrite nanoparticles, like sol-gel, hydrothermal, sol-gel auto-combustion, microwave, combustion, and co-precipitation [16].

Due to the lower reaction time, simplicity, and eco-friendly nature of the co-precipitation method, it was utilized in this project. According to prior explorations, the $ZnFe_2O_4$ had a remarkable function in photocatalytic and magnetic applications. D. Li et al. synthesized spinel $ZnFe_2O_4$ using the sol-gel method [17]. The nickel ferrite nano photocatalyst was synthesized by Hirthna et al., using the chemical co-precipitation method for degrading methyl orange and after 5 h reaction time around 72% of dye were eliminated [18]. However, through the application of the anatase-$ZnFe_2O_4$ nano catalyst prepared by this approach, Andris sutka et al. observed that after about reaction time of 3 h around 96% of methyl orange was decomposed [19].

The photocatalysts method is considered as one of the promising AOPs, which have extensive utilization in contaminant removal from wastewater. Low effectiveness in particular in the case of wastewaters with the high concentered contaminants is one of the major shortcomings of photocatalytic methods. Being a comprehensive investigation of the photocatalytic mineralization

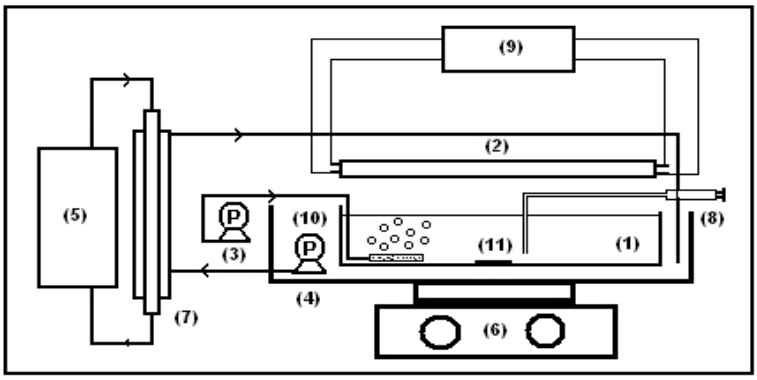

Fig. 1. Schematic diagram of photocatalytic batch reactor:(1- Effluent solution 2- UV lamp 3- Aeration pump 4- Batch reactor, 5-thermo-Bath, 6-magnetic Stirrer, 7-Heat exchanger 8-sampling Point, 9-power supply source 10-Circular pump 11- Magnetic bar).

mechanism of TBA as a recalcitrant contaminant is the innovative prospect of this research.

In this project, through the application of the co-precipitation approach, the nanoparticles of $ZnFe_2O_4$ were synthesized and characterized by SEM, FT-IR and XRD methods. The optimization of crucial operational factors including pH, catalyst dosage and initial TBA concentration for degrading synthetic wastewater, including a certain concentration of TBA through the UV/$ZnFe_2O_4$ have been explored.

EXPERIMENTAL

Material and Apparatus

In this research, an analytical grade of TBA was supplied from Merck Company. The TBA was reduced to enough degree of concentration and utilized in all experiments without any additional adjustment. The other utilized materials were NaOH, HCl, H_2SO_4, $Fe(NO_3)_2.9H_2O$, $FeCl_2$, and $Zn(NO_3)_2.6H_2O$ supplied by Merck, Germany. The SEM evaluations were implemented by JEOL, JSM- 67001. At a diffraction angle from 10° to 80° and using XRD 6000 (Schimadzu model with Cu Kα radiation (λ=0.154 nm) the $ZnFe_2O_4$ nano photocatalyst XRD was logged. The FT-IR device was an IFS 66W Spectrometer model from Bruker. During the research, distilled water was employed.

$ZnFe_2O4$ Preparation

For preparation of the $ZnFe_2O_4$ nano photocatalyst using co-precipitation method, Ferrous nitrate [$Fe(NO_3)_2.9H_2O$] was mixed with a saturated solution of zinc nitrate [$Zn(NO_3)_2.6H_2O$], then NaOH (0.1M) was added dropwise to the solution. Afterward oleic acid surfactant was added to the mixture with certain amount. Through the application of a magnetic stirrer, the mixtures were stirred regularly until reaching a pH value of 12. The final solution was precipitated in an alkaline environment and refluxed for 30 min. Mixture of ethanol and distilled water was used for cleaning the final product and eliminating unsuitable impurities and residual surfactants. After that, the solution was filtered and the precipitate was located in the oven for 2h for drying the products. Finally, the solution was located in a muffle furnace for 5 h at 700 °C and the calcined precipitate was sieved with 100 mesh.

Experimental Design

A UV lamp was located horizontally on the reactor with a 2-liter capacity and for controlling the temperature located in a heat bath (Fig. 1). The UV radiation source was a UV lamp from Philips Company of Holland with following specifications: power = 15 w, length = 50 cm and diameter = 2 cm. This lamp was a low mercury pressure type which shined horizontally over the surface of the solution. The conditions for all sampling were similar, and all the solutions were exposed to ultraviolet light without a dead zone. The catalyst particles were suspended and slightly settled by stirring and aerating. Fig. 1 presents this experimental design.

Overall Procedure

In order to implement the photocatalyst method, a certain concentration of TBA and catalyst were prepared. To reach an equilibrium in the adsorption of TBA molecules on the catalyst surface the sample was placed in the dark reactor for 30 min. The TBA molecules were adsorbed

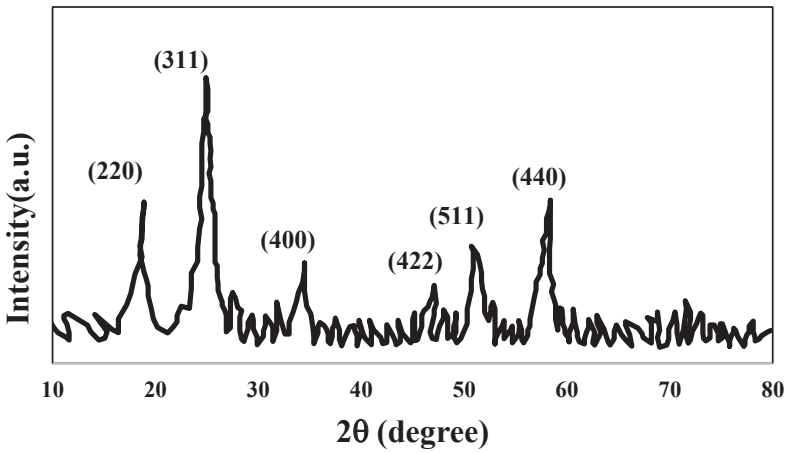

Fig. 2. XRD spectra of $ZnFe_2O_4$ nanoparticles.

on the photocatalyst surface and the quantity of the pollutant was reduced. According to the experimental outcomes, after 30 min in which the lamp was turned off, a considerable reduction in the concentration of the TBA resulted; that is, in the neutral condition, utilizing 0.3 g/L of the catalyst result in 41% absorption in the initial amount of TBA (25 mg/L) on the catalyst surface. After that the lamp was turned on and the reaction was initiated. Through using the thermostat, the temperature was set at 25 °C. Moreover, using a diffuser at the bottom of the reactor O_2 was injected into the solution. In order to avoid any dead space and maintain a homogeneous mixture, by using a stirrer the solution inside the reactor was mixed with O_2. For pH adjustment, the H_2SO_4 solution (0.1 M) was utilized. The sample was conducted at 20 min intervals and for separation of the catalyst particles was centrifuged. The TBA concentration in an aqueous solution was calculated using headspace approach connected to gas chromatography based on DIN 38407-F9-1 (Stationary phase: SGE BP-624 (Ciano-Methyl-Phenylsilicone), Detector: FID).

The solution was exposed to ultra-violet radiation for 120 min. Moreover, based on the related standards, the COD test was utilized. Crucial parameters in the photocatalytic analysis including TBA concentration, catalyst concentration, and pH were explored. The elimination percentage of TBA was given as a function of time according to Eq. 2.

$$\text{TBA Elimination}(\%) = \left(\frac{[\text{TBA}]_0 - [\text{TBA}]_t}{[\text{TBA}]_0} \right) \times 100 \quad (2)$$

Where $[TBA]_0$ and $[TBA]_t$ are the initial concentrations of TBA at times of 0 and t, respectively.

RESULT AND DISCUSSION

Characterization Results

XRD Spectra

Fig. 2 demonstrated the XRD pattern of the $ZnFe_2O_4$ nanoparticles. It is evident that the single phase of cubic spinal crystal construction was generated. Within the circumference of X-ray recognition, the $ZnFe_2O_4$ had no pollution peaks. Based on the wide peaks of XRD, it can be realized that the synthesized particles are in the nanometer range. The crystal planes of spinel $ZnFe_2O_4$ can be indexed by the peaks at the 2θ values of 25.1°, 34.5°, 46.0°, 53.0°, and 57°. Also, sharp peaks were obtained and no considerable movements occurred at the peak position. Nevertheless, decreasing the peak intensity stemmed from the promising generation of certain amorphous construction.

It must be mentioned that using the Debye-Scherer (Eq.3) from the noticeable diffraction peaks, the average crystallite sizes of the $ZnFe_2O_4$ catalyst can be calculated [20].

$$d = K\lambda/\beta\text{Cos}\theta \quad (3)$$

Where λ, the wavelength of the used X-ray, θ is the Bragg angle, β is the Perfect Width at Half-Maximum of the peak (FWHM), and K is equal to 0.9. The average crystalline size was measured to be around 26 nm through using Eq.3 and the X-ray line broadening.

FT-IR Spectra

Fig. 3 presented the FT-IR absorption spectrum of as-prepared $ZnFe_2O_4$ nanoparticles in the

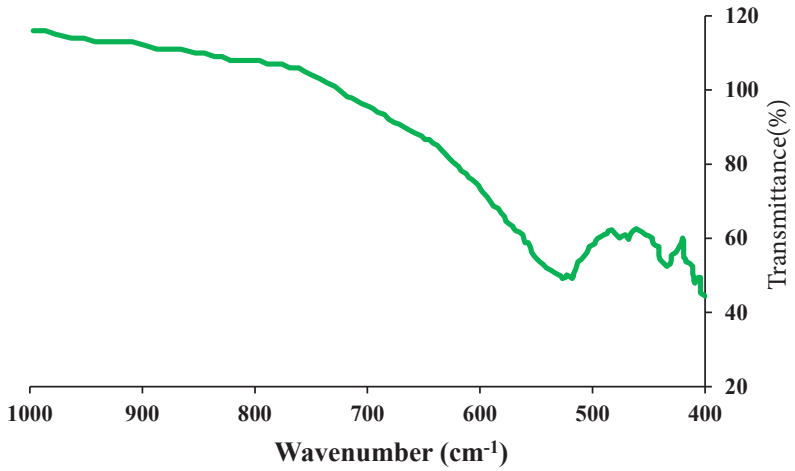

Fig. 3. FT-IR spectra of $ZnFe_2O_4$ nanoparticles.

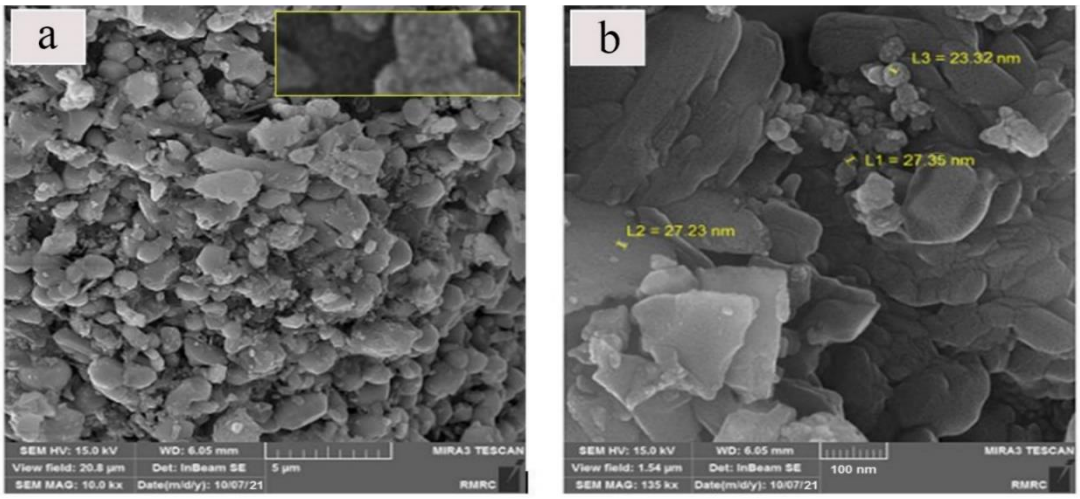

Fig. 4. SEM image of $ZnFe_2O_4$ nanoparticle.

range of 400-4000 cm^{-1}. It was applied to indicate the chemical structure of the contaminant. It was obvious that the FT-IR spectra of all the cubic spinel ferrites generally depict two absorption bands in the range of 400-600 cm^{-1}. The higher frequency band suggests the M-O bond stretching vibrations in the tetrahedral region while the lower frequency indicates the octahedral M-O bond stretching vibrations [21]. The synthesized catalyst demonstrated a peak in the range of 525-540 cm^{-1} matching the stretching vibrations of the M-O clusters in the tetrahedral sites. According to the shifting of peak to lower frequency, the peak correlation with the vibrations in the octahedral sites was not detected in all the morphologies [22-23].

SEM Images

In order to determine the size of distribution and morphology of the $ZnFe_2O_4$ nanoparticles, the SEM images were used. Fig. 4 presented the characteristic SEM images of synthesized $ZnFe_2O_4$. According to the SEM image, the catalyst holds a micrometrical collection of small particles. The existence of free pore crystallite on the surface of the catalyst can be shown by a high dense accumulation. The accumulated form of $ZnFe_2O_4$ was depicted by SEM images. When nanoparticles possess significant surface energies, they cluster and grow into more enormous assemblages. Using SEM image, the kind and size of $ZnFe_2O_4$ particles have been ascertained which are in proper harmony with the dimensions expected to conduct

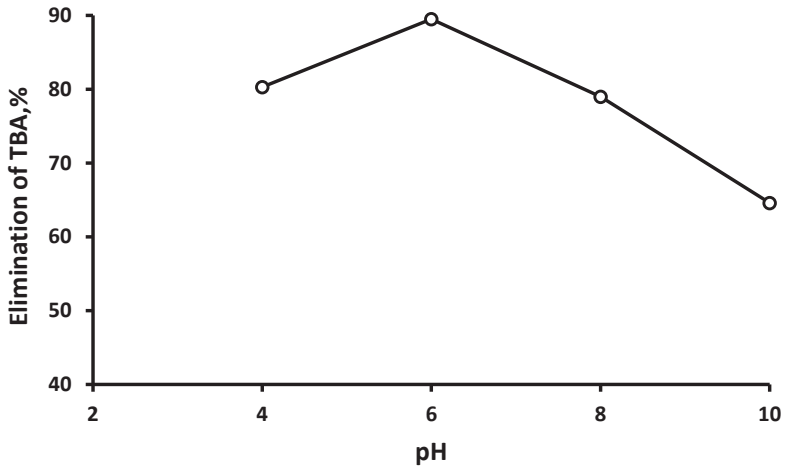

Fig. 5. Influence of pH on the TBA decomposition effectiveness (time at 120 min, catalyst dosage at 1 g/l, and initial dosage of TBA at 30 mg/l).

the process. According to the specified scale, the average particle size of the catalyst was 26 nm.

Determination Method of the Zero-point Charge of $ZnFe_2O_4$ Catalyst

The zero-charge point (ZCP) of catalyst was achieved by the subsequent approaches, around 0.05 g of catalyst was added into eight Erlenmeyer flasks (100 mL) holding $NaNO_3$ solution (0.1 M). Using HNO_3 and NaOH (0.01 $mol.L^{-1}$), pH of the eight containers was controlled at 2, 3, 4, 5, 6, 7, 8, and 9. Then, to reach equilibrium, the solution blends were positioned in an isothermal shaker for 24 h at 25°C. Then, after one day equilibrium the ultimate pH was calculated and the pH of each container where its initial pH was equal to its ultimate pH, presented as the zero-charge point. In this research, the $ZnFe_2O_4$ ZCP was obtained at a pH value of 7 [24].

Influence of pH on the TBA Elimination

The pH has a complex effect on photo-decomposition effectiveness. Due to the influences of pH on the electrostatic force between the contaminant and catalyst, typically, photo-degradation effectiveness is based on the different kinds of contaminant and the zero-charge point of the photocatalyst. The quantity of the adsorbed contaminant on the catalyst surface besides its degradation quantity is significantly close to the catalyst zero-charge point.

For each kind of contaminant, the optimum point of pH is different according to its nature; hence the influence of pH cannot be determined and must be established for each kind of contaminant in the laboratory individually [25]. As a result at established pH, the contaminant charge and catalyst surface, also the attraction and repulsion forces between them must be explored.

As demonstrated in Fig. 5, the photo-degradation of TBA is studied at pH values between 4 and 10. The optimum pH for the degrading contaminants is close to the zero-charge point of the $ZnFe_2O_4$ catalyst. The catalyst ZCP was calculated at almost neutral pH, hence the catalyst surface at pH values lower and higher than neutral was positive and negative, respectively. Different values of pH result in different interaction conditions between the catalyst surface and TBA. The catalyst surface was positive at 6, hence the attraction between the catalyst and TBA was highest with a negative charge and eliminated under experimental situations around 80.5% of TBA. In alkaline environments, OH^- ions were abundant which confirmed the OH^- generation through the photocatalytic process [26].

Moreover, in alkaline environments, since more OH^- is generated from OH^- ions as a result, the radical scavenging effect occurred (Fig. 5) [27]. Hence, at a pH value of 10 in experimental situations, the quantity of TBA decomposition reduced to 60.6%. During all experiments, because of the generation of mineral acids, the pH was decreased slightly throughout the reaction progress. For instance, the initial pH was regulated at 10 at the beginning of remediation and decreased to 8 at the end of the remediation progress.

Influence of Photocatalyst Concentration on the TBA Elimination

To optimize catalyst concentration, experiments

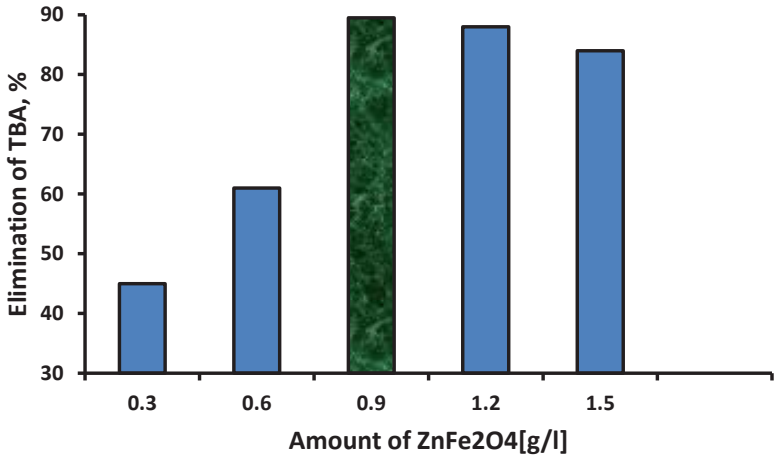

Fig. 6. Influence of catalyst dosage on the degrading TBA (time at 120 min, initial dosage of TBA at 30 mg/l, and pH = 6).

were conducted by varying the catalyst dosage from 0.3 g/l to 1.5 g/l (Fig. 6). The outcomes revealed that through enhancing the quantity of $ZnFe_2O_4$ from 0.3 g/l to 0.9 g/l, the decomposition of TBA after 120 min enhanced from 45% to 89.5%, and then through enhancing the catalyst dosage from 0.9 g/l to 1.2 and 1.5 g/l it was reduced slightly to 88 % and 84%, respectively. These results can explain that enhancing the catalyst concentration will cause increasing hydroxyl and superoxide radicals, the number of electron pairs and positive holes, and the catalyst's active surface [28].

During the first 30 min of the reaction, when the ultra-violet lamp was turned off in all tests and only the adsorption of pollutants on the catalyst was initiated, with an additional enhancement in the quantity of catalyst from 0.3 g/l to 0.6 g/l, the quantity of pollutant elimination enhanced from 45% to 61%, and after that, through an additional enhancement in the quantity of catalyst from 0.9 g/l to 1.5 g/l, the pollutant elimination reduced slightly. The reasons are that rising the catalyst dosage can result in light scattering in the mixture and additional quantities of solid catalyst avoid the penetration of light photons into solution and as a result, decrease the generation rate of $OH^{\cdot}$ [29]. Catalyst particles at higher dosages become accumulated and conglomerated, hence the number of active catalyst centers is decreased [30]. Hence, 0.9 g/l of catalyst was established as the optimum dosage of $ZnFe_2O_4$.

The catalyst should be utilized in the optimum dosage. In the significant dosages of catalyst, because of ambiance turbidity the radiant energy effectiveness reduced. Nevertheless, the optimal dosage of consumed catalyst remarkably is based on the kind and beginning dosage of the contaminant and the ratio of free radical generation. Hence, firstly the needed concentration of catalyst must be determined under the favorable situations on a lab scale, and after that its dosage must be ascertained for a wide range of applications [31-32]. The reactor content must be radiated evenly, which is one of the major challenges in the commercialization of the photocatalytic method [33].

Influence of Initial TBA Dosage on the TBA Elimination

The effect of the initial dosage of TBA from 25 to 100 mg/l was explored on photocatalytic effectiveness (Fig. 7). Through enhancing the initial dosage of TBA, the rate of contaminant decomposition is reduced. At a significant initial TBA dosage (100 mg/l), the number of active centers and generated $OH^{\cdot}$ was decreased since the TBA molecules fought with the catalyst particles to absorb light and after 120 min, just 32.6% of the contaminants were removed. Furthermore, with rising the initial dosage of TBA, they will interact with higher $OH^{\cdot}$, hence the number of radicals and as a result, the elimination effectiveness is reduced [34]. Moreover, more photons were absorbed in the significant dosage of TBA, hence, the TBA decomposition effectiveness was reduced.

The significant dosage of pollutants can perform as catalyst toxins [35]. The photocatalytic process cannot oxidize highly concentrated wastewaters so to overcome this issue they must be diluted. By decreasing the TBA dosage from 100 to 25 mg/l and at optimal empirical situations, the TBA

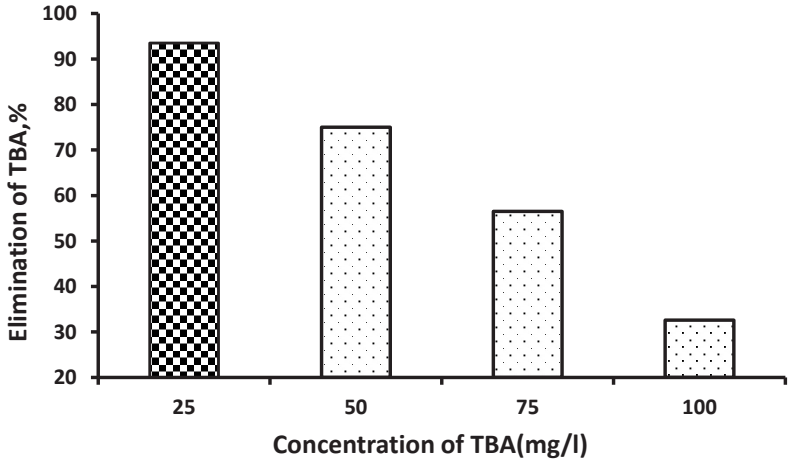

Fig. 7. Influence of initial TBA dosage on photo-decomposition effectiveness (time at 120 min, catalyst dosage at 0.9 g/l and at pH = 6).

elimination raised from 32.6 to 93.5%. Moreover, the Langmuir-Hinshelwood model can be applied to associate the reaction rate to the initial dosage of TBA, however, the factors of this model significantly rely on the operational circumstances and effluent structure [36].

The Function of O_2 in the UV/$ZnFe_2O_4$

The existence of oxygen or other oxidizing species results in a remarkable increase in the photo-decomposition of organic matters. In numerous photocatalytic methods, the light-produced electrons in the conduction band of the catalyst surface can react with the adsorbed oxygen which causes the generation of superoxide radicals ($O_2^{-\bullet}$)Hence, unfavorable effects of electron-hole recombination were avoided (Eq.10) [37]. The reaction of superoxide radicals with building atoms and organic matters results in the degradation of the contaminants into CO_2 and H_2O. Because in the photocatalyst process, the transformation of an electron to O_2 is the rate-controlling factor. Hence, in this work by a shallow selection of the solution inside the reactors, providing oxygen by the capsule and stirring, the influence of O_2 dosage in the determination of speed was eliminated. The holes in the valence band (VB) oxidize the water molecules and the OH^- ions adsorbed on the catalyst surface and generate $OH^{\cdot}$. The oxidation of contaminant molecules might occur either directly by the positive cavities of the VB before it is trapped inside or at the particle surface or indirectly, by attachment of OH^- to the surface (Eqs.7 and 8). The generated $O_2^{-\bullet}$ from Eq.10 might generate H_2O_2 (Eq.11) and, using UV irradiation, separate oxygenated water to form an $OH^{\cdot}$ that reacts with the intermediate constituents to generate final products (Eq.9) [38].

$$ZnFe_2O_4 + hv \rightarrow h^+_{vb} + e^-_{CB} \quad (4)$$

$$h^+_{vb} + e^-_{CB} \rightarrow \text{heat} \quad (5)$$

$$h^+_{vb} + TBA \rightarrow \text{intermediates} \rightarrow CO_2 + H_2O \quad (6)$$

$$h^+_{vb} + H_2O\ (ads) \rightarrow OH^{\bullet}_{ads} + H^+ \quad (7)$$

$$h^+_{vb} + OH^-_{ads} \rightarrow OH^{\bullet}_{ads} \quad (8)$$

$$OH^{\bullet}_{ads} + TBA_{(ads)} \rightarrow \text{ntermediates} + OH^{\bullet}_{ads} \rightarrow CO_2 + H_2O \quad (9)$$

$$e^-_{CB} + O_2 \rightarrow O_2^{-\bullet} \quad (10)$$

$$O_2^{-\bullet} + OH^{\bullet} + H^+ \rightarrow O_2 + H_2O_2 \quad (11)$$

COD Elimination Effectiveness

As demonstrated in Fig. 8, because of the adsorption of contaminant molecules on the catalyst surface, around 10 % and 25.5% of the COD was eliminated after 20 and 40 min from the process initiated when the ultra-violet lamp was turned off. With the inception of light radiation and beginning the reaction, the COD rate reduced since the molecules adsorbed on the catalyst surface started to collapse and generate intermediate matters including COD. By the progress of the reaction, these intermediates were again attacked by $OH^{\cdot}$ which finally, converted them to compounds like CO_2 and H_2O.

The ratio of COD stem from 25 mg/l of TBA at optimal situations was 100 mg/l. During optimum situations of the TBA decomposition process, even though 93.5% of the pollutants were eliminated,

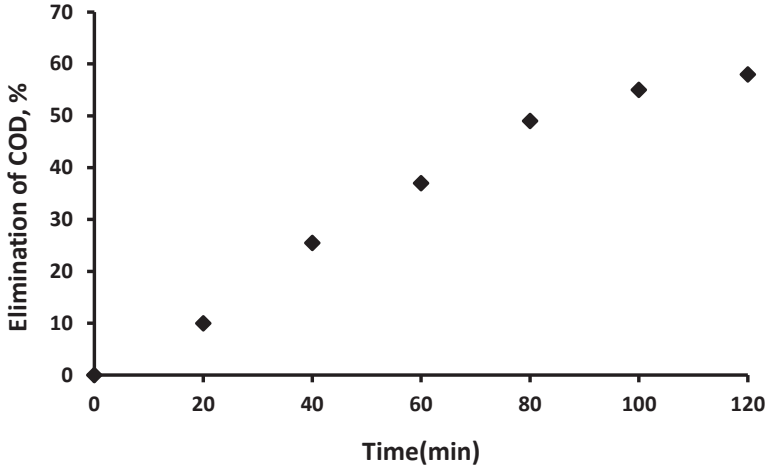

Fig. 8. COD elimination in degrading of TBA under optimum situations (120 min of reaction time, the catalyst dosage at 0.9 g/l and pH = 6).

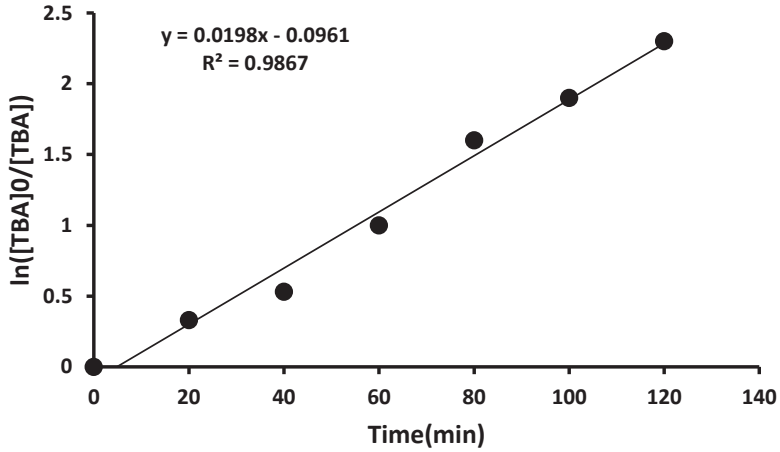

Fig. 9. Constant rate reaction of TBA decomposition under optimum situations (pH = 6, initial dosage of TBA at 25 mg/l and catalyst dosage at 0.9 g/l).

just 58% of the COD was eliminated, which implies the generation of intermediate compounds and the unfinished TBA degradation [39].

Investigating Photo-degradation Reaction Kinetic

In order to elucidate the kinetics of the photo-decomposition reaction in the aqueous medium, the Langmuir-Hinshelwood model was utilized. As presented in Eq.12, this model heavily relies on the TBA concentration (C_{TBA}) and the TBA decomposition rate (R_{TBA})

$$R_{TBA} = \frac{k_r K_{ad} C_{TBA}}{1 + K_{ad} C_{TBA}} \quad (12)$$

Where K_{ad} is the absorption equilibrium constant on the photocatalyst surface and kr is the reaction rate constant. In this work, the adsorption of TBA on the catalyst surface was insignificant, and, in optimum situations, a low dosage of TBA (25 mg/l) was utilized, as a result, Eq.11 was simplified and converted to a pseudo-first-order kinetic equation below with an apparent k_{app} rate constant.

$$R_{TBA}=k_r K_{ad} C_{TBA}=k_{app} C_{TBA} \quad (13)$$

According to the experimental outcomes, reaction rate constants were achieved utilizing laboratory data and pseudo-first-order reaction rate equations, and these results were in agreement with the findings of different researchers [40-41]. After integration of Eq.13, Eq.14 is achieved.

$$\ln\left(\frac{[TBA]_0}{[TBA]_t}\right) = K_{app} \times t \qquad (14)$$

Where $[TBA]_0$ and $[TBA]_t$ are the concentration of TBA at the initial of the reaction and time t, respectively. In order to assess these rate constants, based on the reaction time (Fig. 9), the expression $\left(\ln\left(\frac{[TBA]_0}{[TBA]_t}\right)\right)$ was outlined, and after exploring the linear regression, the half-life of the reaction and the pseudo-first-degree rate constant, ($t_{1/2}$=35 min) and (K_{app}=1.98×10^{-2} min^{-1}) were obtained.

CONCLUSION

Through using the co-precipitation method, the catalyst nanoparticles were synthesized and characterized by SEM image, XRD and FT-IR spectroscopy. Using FTIR and XRD spectrum, it was detected that the nano catalyst had a cubic spinel structure. The average particle size of the catalyst was 26 nm.

For degradation of TBA in batch reactors which substantially relies on pH, initial TBA concentration, and catalyst concentration, the UV/$NiFe_2O_4$ method was utilized. Optimum situations in the TBA mineralization were determined as pH at 6, 25 mg/l of TBA, and 0.9 g/l of catalyst. Around 58% of COD and 93.5% of TBA were eliminated which implies the generation of intermediate-recalcitrant matters and the unfinished degradation of TBA.

The electron-hole mechanism is the reason for the generation of active radicals in the photocatalyst method. Because of the decreasing number of received photons on the catalyst surface and the light scattering phenomenon, with enhancing the photocatalyst dosage higher than a specific degree, the photocatalytic effectiveness was decreased.

According to the Langmuir model, the kinetics of the TBA mineralization were elucidated and the half-life of the reaction and the pseudo-first-degree rate constant, were obtained ($t_{1/2}$=35 min) and (K_{app}=1.98×10^{-2} min^{-1}), respectively.

CONFLICT OF INTEREST

The authors declare no conflicts of interest.

REFERENCES

[1] M. Cai, X. Wang, Y. Mo, Y. Chen, L. Dai, Microporous Mesoporous Mater. 333:111725 (2022). https://doi.org/10.1016/J.MICROMESO.2022.111725.
[2] J. Isanapong, P. Pornwongthong, J. Hazard. Mater. 411:125104 (2021). https://doi.org/10.1016/J.JHAZMAT.2021.125104.
[3] D. Dobslaw, J. Schöller, D. Krivak, S. Helbich, K.H. Engesser, Chem. Eng. J. 355: 572 (2019). https://doi.org/10.1016/J.CEJ.2018.08.140.
[4] A. Toumari, I.H. Suffet, Int. J. Environ. Sci. Technol. 18:2879 (2021). https://doi.org/10.1007/S13762-020-03041-Z.
[5] Aerob. Util. Hydrocarb. Oils, Lipids. (2019). https://doi.org/10.1007/978-3-319-50418-6.
[6] S. Saponaro, M. Negri, E. Sezenna, L. Bonomo, C. Sorlini, J. Hazard. Mater. 167:545 (2009). https://doi.org/10.1016/J.JHAZMAT.2009.01.026.
[7] R. Schmidt, D.A. Klemme, K. Scow, K. Hristova, J. Hazard. Mater. 209:524 (2012). https://doi.org/10.1016/J.JHAZMAT.2012.01.057.
[8] M. Mehrjouei, S. Müller, D. Möller, Chem. Eng. J. 211:353 (2012). https://doi.org/10.1016/J.CEJ.2012.09.079. https://doi.org/10.1016/j.cej.2012.09.079
[9] K. Li, D.R. Hokanson, J.C. Crittenden, R.R. Trussell, D. Minakata, Water Res. 42:5045 (2008). https://doi.org/10.1016/J.WATRES.2008.09.017. [10] T. Garoma, M.D. Gurol, O. Osibodu, L. Thotakura, Chemosphere. 73:825 (2008). https://doi.org/10.1016/J.CHEMOSPHERE.2008.06.061. https://doi.org/10.1016/j.chemosphere.2008.06.061
[11] A.R. Khataee, M.B. Kasiri, J. Mol. Catal. A Chem. 8:328 (2010). https://doi.org/10.1016/J.MOLCATA.2010.05.023. [12] A. Shokri, K. Mahanpoor, D. Soodbar, Fresenius Environ. Bull. 25:500 (2016). https://www.sid.ir/en/Journal/ViewPaper.aspx?ID=521657.
[13] A. Shokri, Int. J. Nano Dimens. 7:160 (2016). https://www.sid.ir/en/Journal/ViewPaper.aspx?ID=506544.
[14] A. Shokri, Environ. Challenges. 5:100332 (2021). https://doi.org/10.1016/j.envc.2021.100332.
[15] A. Lassoued, M.S. Lassoued, B. Dkhil, S. Ammar, A. Gadri, J. Mater. Sci. Mater. Electron. 29:7057 (2018). https://doi.org/10.1007/S10854-018-8693-0.
[16] J. He, S. Yang, A. Riisager, Catal. Sci. Technol. 8:790 (2018). https://doi.org/10.1039/C7CY02197F.
[17] D.Y. Li, Y.K. Sun, P.Z. Gao, X.L. Zhang, H.L. Ge, Ceram. Int. 40:16529 (2014). https://doi.org/10.1016/J.CERAMINT.2014.08.006.
[18] Hirthna, S. Sendhilnathan, P.I. Rajan, T. Adinaveen, J. Supercond. Nov. Magn, 31:3315 (2018). https://doi.org/10.1007/S10948-018-4601-3.
[19] A. Šutka, M. Millers, N. Döbelin, R. Pärna, M. Vanags, M. Maiorov, J. Kleperis, T. Käämbre, U. Joost, E. Nõmmiste, V. Kisand, M. Knite, Phys. Status Solidi. 212:796 (2015). https://doi.org/10.1002/PSSA.201431681.
[20] A. Shokri, Surfaces and Interfaces. 21:100705 (2020). https://doi.org/10.1016/J.SURFIN.2020.100705.
[21] H. Moradmard, S. Farjami Shayesteh, P. Tohidi, Z. Abbas, M. Khaleghi, J. Alloys Compd. 650:116 (2015). https://doi.org/10.1016/J.JALLCOM.2015.07.269.
[22] A.M. Dumitrescu, G. Lisa, A.R. Iordan, F. Tudorache, I. Petrila, A.I. Borhan, M.N. Palamaru, C. Mihailescu, L. Leontie, C. Munteanu, Mater. Chem. Phys. 156:170 (2015). https://doi.org/10.1016/J.MATCHEMPHYS.2015.02.044.
[23] V.S. Sawant, A.A. Bagade, S.V. Mohite, K.Y. Rajpure, Phys.B451(2014)39-42. https://doi.org/10.1016/j.physb.2014.06.019

[24] A. Shokri, M. Salimi, T. Abmatin, Fresenius Environ. Bull. 26:1560 (2017).
[25] O.D. Arefieva, M.S. Vasilyeva, I. V. Lukiyanchuk, E.S. Sedinkina, L.A. Zemnukhova, A.I. Pisartseva, Russ. J. Inorg. Chem. 66:943 (2021). https://doi.org/10.1134/S0036023621060036.
[26] H.A. Kiwaan, T.M. Atwee, E.A. Azab, A.A. El-Bindary, J. Mol. Struct. 1200:127115 (2020). https://doi.org/10.1016/J.MOLSTRUC.2019.127115.
[27] A.H. Zyoud, A. Zubi, S.H. Zyoud, M.H. Hilal, S. Zyoud, N. Qamhieh, A.R. Hajamohideen, H.S. Hilal, Appl. Clay Sci. 182:105294 (2019). https://doi.org/10.1016/J.CLAY.2019.105294.
[28] M.F. Hanafi, N. Sapawe, Mater. Today Proc. 31:318 (2020). https://doi.org/10.1016/J.MATPR.2020.06.066.
[29] M. Saghi, A. Shokri, A. Arastehnodeh, M. Khazaeinejad, A. Nozari, J. Nanoanalysis. 5:163 (2018). https://doi.org/10.22034/JNA.2018.543608.
[30] M. Rostami, A. Hassani Joshaghani, H. Mazaheri, A. Shokri, Int. J. Eng. Trans. A Basics. 34:756 (2021). https://doi.org/10.5829/ije.2021.34.04a.01.
[31] M. Rostami, H. Mazaheri, A. Hassani Joshaghani, A. Shokri, Int. J. Eng. Trans. B Appl. 32:1074 (2019). https://doi.org/10.5829/ije.2019.32.08b.03.
[32] N.S. Alharbi, B. Hu, T. Hayat, S.O. Rabah, A. Alsaedi, L. Zhuang, X. Wang, Front. Chem. Sci. Eng. 14:1124 (2020). https://doi.org/10.1007/S11705-020-1923-Z.
[33] R. Gusain, K. Gupta, P. Joshi, O.P. Khatri, Adv. Colloid Interface Sci. 272:102009 (2019). https://doi.org/10.1016/J.CIS.2019.102009.
[34] X. Zhang, J. Wang, X.X. Dong, Y.K. Lv, Chemosphere. 242:125144 (2020). https://doi.org/10.1016/J.CHEMOSPHERE.2019.125144.
[35] A. Nezamzadeh-Ejhieh, M. Amiri, Powder Technol. 235:279 (2013). https://doi.org/10.1016/J.POWTEC.2012.10.017.
[36] S. Pourfalatoon, H. Mazaheri, A. Hassani Joshaghani, A. Shokri, Iran. J. Chem. Chem. Eng. 40:804 (2021). https://doi.org/10.30492/IJCCE.2020.38105.
[37] R. Hekmatshoar, A.R. Yari, A. Shokri, J. Nanoanalysis. 7:282 (2020). https://doi.org/10.22034/jna.
[38] B. Xia, F. Deng, S. Zhang, L. Hua, X. Luo, M. Ao, J. Hazard. Mater. 392:122345 (2020). https://doi.org/10.1016/J.JHAZMAT.2020.122345.
[39] B. Ye, Y. Li, Z. Chen, Q.Y. Wu, W.L. Wang, T. Wang, H.Y. Hu, Water Res. 124:381 (2017). https://doi.org/10.1016/J.WATRES.2017.05.059.
[40] A. Mirzaei, L. Yerushalmi, Z. Chen, F. Haghighat, J. Hazard. Mater. 359:516 (2018). https://doi.org/10.1016/J.JHAZMAT.2018.07.077.
[41] M.S.F.A. Zamri, N. Sapawe, Mater. Today Proc. 19:1261 (2019). https://doi.org/10.1016/J.MATPR.2019.11.131.